Highly conductive ZnO films with high NIR transparency

M. Hála[1,*], S. Fujii[2], A. Redinger[1], Y. Inoue[2], G. Rey[1], M. Thevenin[1], V. Deprédurand[1], T. P. Weiss[1], T. Bertram[1], S. Siebentritt[1]

[1)] Laboratory for Photovoltaics, Physics and Materials Science Research Unit, Université du Luxembourg, 41, rue du Brill, L-4422 Belvaux, Luxembourg

[2)] TDK Corporation Technical Center, 2-15-7, Higashi Owada, Ichikawa, Chiba, 272-8558 Japan

[*)] email: matej.hala@uni.lu

Abstract We present an approach for deposition of highly conductive nominally undoped ZnO films that are suitable for the n-type window of low band gap solar cells. We demonstrate that the low-voltage radio frequency (RF) biasing of the growing ZnO films during their deposition by non-reactive sputtering makes them as conductive as when doped by aluminium ($\rho \leq 1 \cdot 10^{-3}\,\Omega\,\mathrm{cm}$). The films prepared with additional RF biasing possess lower free carrier concentration and higher free carrier mobility than the Al-doped ZnO (AZO) films of the same resistivity, which results in a substantially higher transparency in the NIR spectral region. Furthermore, these films exhibit good ambient stability, and lower high temperature stability than the AZO films of the same thickness. We also present the characteristics of $Cu(InGa)Se_2$, $CuInSe_2$ and $Cu_2ZnSnSe_4$-based solar cells prepared with a transparent window bilayer formed of the isolating and conductive ZnO films, and compare them to their counterparts with a standard ZnO/AZO bilayer. We show that the solar cells with nominally undoped ZnO as their TCO layer exhibit an improved quantum efficiency for $\lambda > 900\,\mathrm{nm}$ which leads to a higher short circuit current density J_{SC}. This aspect is specifically beneficial in preparation of $Cu_2ZnSnSe_4$ solar cells with band gap down to 0.85 eV; our champion device reached a J_{SC} of nearly $39\,\mathrm{mA\,cm^{-2}}$, an open circuit voltage of 378 mV, and a power conversion efficiency of 8.4 %.

I. INTRODUCTION

Thin film solar cells based on $Cu(InGa)Se_2$ or $Cu_2ZnSn(S,Se)_4$ are usually made with an n-type window consisting of an undoped ZnO layer and the ZnO:Al (AZO) layer [1], including recent record efficiency devices [2–5]. AZO is an almost ideal transparent conductive oxide (TCO) material for a window layer in thin film solar cells: it is non-toxic, highly transparent in the visible and NIR regions, and it can be made highly conductive [6]. However, some rather low band gap solar cell materials (with E_g around 1 eV) have recently come into focus, such as pure selenide $Cu_2ZnSnSe_4$ [7–9] and also pure $CuInSe_2$ [10, 11] which is of interest as a bottom partner in a tandem cell [12–14]. For such materials the short circuit current is reduced by free carrier absorption in the AZO layer, which starts to reduce the transmission from about 900 nm wavelength on upwards.

Therefore, it is advisable to replace the AZO layer by an alternative with a higher plasma wavelength λ_p (and thus better transparency in NIR) while retaining a high conductivity. This can be achieved by increasing the carrier mobility and lowering the carrier effective mass; There are several candidates that can satisfy these requirements, such as more expensive In_2O_3:Sn (ITO), In_2O_3:Ti (ITiO), In_2O_3:Mo (IMO) [6, 15], or ZnO:B [16]. An alternative option for improving the carrier mobility is the preparation of a superlattice layer consisting of stacked lightly and heavily doped TCO materials, such as $ZnO/Zn_{1-x}Mg_xO$ stacks [17, 18]. However, this would increase the complexity of the deposition process. Another possibility to raise λ_p is to tune the dielectric permittivity of the TCO window through the judicious doping by a high-permittivity material (e.g., ZrO_2) [19].

An important TCO candidate to be also considered is the unintentionally doped ZnO that can exhibit resistivity comparable to AZO due to deviations from zinc/oxygen stoichiometry [18]. First reports on highly conductive and transparent ZnO layers date back to the early eighties, when films of resistivities ρ as low as $5 \cdot 10^{-4}\,\Omega\,\mathrm{cm}$ were obtained by magnetron sputtering technique under the conditions of plasma exposure to the growing film [20]. A drop in ρ was achieved by either a solenoid positioned close to the samples which guided the magnetized plasma from the magnetron [20, 21], or by an additional radio frequency (RF)-powered discharge operated above sample's surface [22–24]. Nevertheless, the latter approach has been mostly disregarded and it has never been considered as a TCO window layer for solar cell fabrication, most probably due to the lower environmental stabil-

ity of nominally undoped ZnO in comparison to AZO [6]. However, the undoped ZnO films prepared by atmospheric pressure plasma-enhanced chemical vapor deposition (PECVD) and turned conductive by post-deposition exposure to near-ultraviolet light were recently reported as suitable to replace the AZO layer as a front electrode in $Cu(InGa)Se_2$ cells, if encapsulated by thin Al_2O_3 overlayer [25].

In the current study we explore the application of the RF substrate biasing in preparation of highly conductive ZnO layers by non reactive sputtering from a ceramic ZnO target. First, we investigate the optimal process conditions that can be used in preparation of stable ZnO films exhibiting as low resistivity as standard AZO films. Afterwards, we discuss their electrical, optical and structural characteristics. We also present the results of the ambient and elevated temperature stability monitoring. Finally, we demonstrate the use of highly conductive nominally undoped ZnO layers within the n-type window of solar cells based on $Cu(InGa)Se_2$, $CuInSe_2$ and $Cu_2ZnSnSe_4$ absorbers, and compare the parameters and performance of these devices with their counterparts fabricated with an AZO layer.

II. EXPERIMENTAL DETAILS

A. Sample preparation

The TCO deposition experiments were performed in a commercial semi-automated sputtering deposition system. Two of the magnetron guns equipped with ceramic 5 cm diameter ZnO and ZnO:Al (2 wt% of Al) targets were powered by either 300 W or 600 W RF generators and operated in non-reactive Ar atmosphere using a constant Ar flow, $\Phi(\mathrm{Ar}) = 25\,\mathrm{sccm}$, and a throttle valve for pressure adjustemnt. In the deposition of non-conductive ZnO (i-ZnO) and conductive ZnO:Al (AZO) films the power load at the target, P, was fixed to 125 W and 140 W, respectively. Instead, in the preparation of conductive "RF-biased" ZnO (b-ZnO) films the power was varied in the range of 60 W to 125 W, as specified for each experiment.

The substrates, soda lime glass (SLG) or CdS-covered solar cell absorbers, were positioned at a distance of 13 cm on a rotatable unheated substrate holder that was optionally biased by an additional RF generator. In such experiments, the self-induced negative DC voltage on the RF-powered substrate holder, U_b (also labelled in this work as RF bias voltage), was

modified in the range from 0 V to 50 V by application of an RF signal to the substrate holder employing low powers ($P < 4$ W, corresponding to power densities below 0.03 W/cm^{-2}). The thickness t of the b-ZnO and AZO films was kept constant at $t \approx 385 \pm 10$ nm.

In the solar cells fabrication experiments two different types of bilayer stacks were prepared, composed of either ZnO ($t \approx 80$ nm) and AZO ($t \approx 385$ nm) films, or ZnO ($t \approx 80$ nm) and b-ZnO ($t \approx 385$ nm, using $P = 125$ W and $U_b = 25$ V) films. These were deposited in a subsequent manner onto underlying Cu(In,Ga)Se_2, $CuInSe_2$ and $Cu_2ZnSnSe_4$ absorbers covered by 60 nm thick CdS buffer layers prepared by chemical bath deposition (CBD). It should be stressed that we used the same CBD recipe for all three absorber types and for all the window stacks under investigation. Subsequently, the cells were finished by electron beam evaporation of Ni-Al contact grids on top of the TCO window. The resulting solar cell area is approximately 0.5 cm^2, as defined by mechanical scribing and verified by optical microscopy. In addition, some of the cells were capped with an antireflective coating made of 100 nm thick MgF_2 layer, also using electron beam evaporation.

Cu(In,Ga)Se_2, $CuInSe_2$ and $Cu_2ZnSnSe_4$ absorbers were prepared in a molecular beam epitaxy system operated at a base pressure of roughly $1{\cdot}10^{-8}$ Torr. The system is equipped with Cu, In, Ga, Sn, Zn and SnSe effusion cells and selenium is supplied through a valved cracker source. The absorbers were deposited by high temperature coevaporation on molybdenum coated soda lime glass. The substrate temperature was controlled with a pyrometer monitor. In addition, the laser light scattering technique was used for end point detection in the case of Cu(In,Ga)Se_2 deposition [26], and for determination of Sn incorporation in the case of $Cu_2ZnSnSe_4$ [27].

Cu-poor Cu(In,Ga)Se_2 (Cu/(Ga+In)< 1) absorbers were grown with the well documented three stage process [28, 29] in order to test the TCO on commercially relevant material. The composition of the absorber, as measured with energy dispersive X-Ray (EDX) analysis, is Cu/(In+Ga) = 0.91 and In/(In+Ga) = 0.29. Furthermore, Cu-rich $CuInSe_2$ (Cu/In > 1) absorbers were prepared via single stage high temperature coevaporation, as detailed in reference [30]. In short, the absorbers is first grown under Cu excess to form a Cu_xSe secondary phase on top of the absorber. Afterwards, this secondary phase is removed by an etching step using potassium cyanide (10 wt% KCN during 5 minutes at room temperature). $Cu_2ZnSnSe_4$ absorbers were grown via multiple stage coevaporation as described in reference [27]. The composition of the latter samples was chosen to be Cu-poor (Cu/(Zn+Sn) <1) and slightly

Zn-rich ($\mathrm{Zn/Sn} > 1$).

B. Sample characterization

First, the film thickness was measured with a profilometer for each TCO sample, and the corresponding resistivity ρ was determined using a homebuilt four point probe Van-der-Pauw setup [31]. Afterwards, the corresponding optical properties were analysed with a spectrophotometer; transmittance ($T(\lambda)$) and reflectance ($R(\lambda)$) were measured and the band gap of the films was subsequently deduced from Tauc's plot. The absorption coefficient $\alpha(\lambda)$ was enumerated using the following formula [32]:

$$\alpha = -\frac{1}{t} \ln\left(\frac{R - r}{r\,T}\right) \tag{1}$$

where r is defined as:

$$r = \frac{(T^2 + 2) - (R-1)^2}{2\,(2-R)} - \sqrt{\left\{\frac{(T^2 + 2) - (R-1)^2}{2\,(2-R)}\right\}^2 - \frac{R}{2-R}}. \tag{2}$$

In order to obtain the plasma wavelength the complex refractive index was first extracted from T and R data, according to the method provided in reference [33], and the corresponding optical constant spectra were subsequently fitted using the Drude model [34].

The crystallinity and the lattice strain of the TCO films were investigated by X-Ray diffractometry (XRD) in $\theta - 2\theta$ geometry using the Cu Kα radiation; the light coherence length was evaluated from the broadening of the ZnO (002) diffraction peak using the Scherrer formula [35], and the lattice strain was calculated as the elongation of the c lattice parameter of wurtzite ZnO cell (also using the ZnO (002) diffraction peak) with respect to its bulk counterpart ($c_{\mathrm{bulk}} = 5.207\,\mathrm{nm}$ [36]).

Chemical composition of the selected samples was analysed by energy dispersive X-ray spectrometry (EDX) using the electron acceleration voltage of 7 keV. Furthermore, secondary-ion mass spectrometry (SIMS) was employed to study the in-depth distribution of Zn, O, Al and Cu in the films. In addition, hydrogen concentration was estimated by SIMS optimised in term of sensitivity by analysing H as negative ion under Cs^+ bombardment (impact energy of 1 keV). Since the composition of b-ZnO and AZO samples under investigation were similar (identical matrix), H signals were directly comparable. Finally, the surface composition was studied by X-ray photoelectron spectroscopy (XPS) using a monochromatic Al Kα radition. For aluminium quantification, the spectra were acquired with the highest sensitivity achievable with the system (the detection limit around 0.2 at.%): the X-ray gun was operated at 150 W and the pass energy of the analyser was fixed at 160 eV.

Completed solar cells have been characterized in a homebuilt current-voltage setup equipped with a cold mirror halogen lamp adjusted to a light intensity of 1000 W/m^2. Their external quantum efficiency (QE) was also measured in the wavelength range of 300 nm to 1600 nm, in order to analyse the variations in spectral response for solar cells with different TCO windows. The solar cell parameters were then obtained with the IV-FIT routine [37] in which a 1-diode model is used to extract the parasitic resistances, the diode quality factor and the reverse saturation current density.

III. RESULTS AND DISCUSSION

A. Optimization of deposition conditions of conductive ZnO films

Magnetron sputtering is a deposition technique commonly used in ZnO fabrication because of its low cost, simplicity, and low operating temperature. In this section we explore the process parameter space resulting in highly conductive nominally undoped b-ZnO films that are prepared under conditions of substrate RF biasing. The ultimate goal of such study is to identify the set of deposition conditions at which the lowest conductivity of b-ZnO films is achieved.

The individual variables that were identified as key parameters and thus investigated are the negative bias voltage caused by the RF power applied at the substrate, U_b, and the power applied to the sputtered target P. Another important deposition parameter of which

effect was examined is the working gas pressure p (varied within the range of 0.05 to 1 Pa). However, it has been found that the film resistivity was the lowest at $p = 0.13$ Pa independently of the used U_b and P combination (results not shown). For this reason, the pressure was a fixed parameter in the experiments presented in Fig. 1.

It is to be noted that all b-ZnO films under investigation were crystalline and highly textured with the c-axis oriented perpendiculary to the substrate surface, as indicated by the pronounced ZnO (002) and (004) XRD diffraction peaks. The only exceptions were the films prepared at the highest substrate bias voltage, $U_b \geq 50$ V, or at the lowest pressure $p = 0.05$ Pa (characterized by the lowest growth rate and thus the highest ion-to-neutral atomic arrival ratio). These latter observations are fingerprints of the excessive ion bombardment-induced damage of the growing layer that has a detrimental effect on resulting film crystallinity.

Figures 1(a-c) show results of the experiments in which P was fixed to 125 W while the U_b was varied from 0 V (substrate floating) to 50 V. In contrast, U_b was fixed to 25 V and the P was varied from 125 W down to 60 W in the experiments depicted in figures 1(d-f). Each data point represents the characteristics of the b-ZnO film that has been prepared using a selected combination of U_b and P.

Figure 1(a) illustrates that the b-ZnO film resistivity plotted as a function of the RF bias voltage exhibits a drop from a very high value that is out of measurement limits of our four-point probe ($\rho > 1 \cdot 10^{+3}\,\Omega$ cm at $U_b = 0$ V, not shown), down to $\rho \approx 1 \cdot 10^{-3}\,\Omega$ cm at $U_b = 25$ V. It is to be stressed that such a low resistivity is identical to that of AZO films prepared under comparable experimental conditions (also highlighted in Fig. 1(a)). Application of lower or higher voltages does not further improve film resistivity that slightly increases in either direction. This observation can be understood if considering the trends in free carrier concentration and mobility, which can be inferred from the evolution of the optical band gap and of the X-ray coherence length, respectively.

Optical band gap values E_g are plotted in Fig. 1(b). The observed rise in E_g from 3.24 eV ($U_b = 0$ V) up to 3.47 eV ($U_b = 31$ V) is consequence of an increasing unintentional doping of ZnO. In fact, this is the effect of the Burstein-Moss shift that reflects a growing charge carrier occupation of the lowest conduction band energy states [38, 39]. Identical trend was also noted for the NIR absorption coefficient (with a maximum at $U_b = 31$ V, results not presented), which is an indicative of intraband absorption caused by an elevated

density of free electrons. Therefore, it can be concluded that the ZnO films biased to $U_b = 25 - 37\,V$ exhibit a significantly enhanced free carrier concentration that peaks at $U_b = 31\,V$. Nevertheless, this concentration has to be considerably lower than in AZO films, as suggested by the respective E_g values ($E_g = 3.47\,eV$ in comparison with $3.74\,eV$) and as discussed in section III B.

Finally, figure 1(c) shows that the X-ray coherence length increases for low U_b up to its peak at 27.5 nm (at $U_b = 25\,V$), and that it drops abruptly down to 9 nm at $U_b = 37\,V$. The decreasing light coherence length is an indicative of the diminishing distance between homogeneously distributed structural defects in perpendicular direction to a substrate surface. This can be directly correlated to an increasing density of structural imperfections (e.g., grain boundaries) that represent possible scattering centres [40]. In addition, a higher level of structural defects is also predicted by an important increase of the lattice strain; a 2-fold rise was observed when U_b was raised from 25 V to 37 V (data not shown). Both of these latter findings suggest an increased scattering experienced by free carriers at $U_b > 25\,V$, an effect that can decrease their mobility and thus cause the rise in film resistivity illustrated in Fig. 1(a). Indeed, it has been documented previously that the free carrier mobility is limited by grain boundary scattering, alongside the ingrain scattering mechanisms (e.g., ionized impurity scattering), in highly conductive SnO_2 [40] and ZnO [21, 25] films.

The experiments in which the RF bias voltage was fixed at $U_b = 25\,V$ but the discharge power was altered from 125 W down to 60 W are depicted in Figures 1(d-f). It is shown that the film resistivity changes only a little with P in contrast to the previous experiments, and that it exhibits a pronounced minimum at 90 W, as visible in the insert of Fig. 1(d). In the following paragraph it will be discussed that these relatively small variations can be interpreted in the same manner as above, by considering the trends in the optical band gap and the X-ray coherence length.

It can be seen that the decrease of sputtering power below 125 W increases slightly the optical band gap, from 3.43 eV at $P = 125\,W$ up to 3.49 eV at low powers (Fig. 1(e)). Instead, the X-ray coherence length first increases up to 30 nm if P is lowered from 125 W to 100 W, and then it decreases for $P < 80\,W$ (Fig. 1(f)). In the similar fashion, the lattice strain exhibits a steady value for $90\,W < P < 125\,W$ and a substantial rise for $P < 80\,W$ (data not shown). The drop in film resistivity, from $\rho = 10.6 \cdot 10^{-4}\,\Omega\,cm$ at $P = 125\,W$ down to $\rho = 8.5 \cdot 10^{-4}\,\Omega\,cm$ at $P = 90\,W$, may thus be understood in terms of a bit

higher concentration of charge carriers (indicated by E_g) and a better charge carrier mobility (suggested by a higher X-ray coherence length). In contrast, the rising value of ρ at lower powers than 90 W is most probably caused by the rising charge carrier scattering due to a higher density of crystallographic defects.

It is to be stressed that the differences in ρ values related to sputtering power alteration are well reproducible and also higher than the process-to-process variations. (This is illustrated in the insert of Fig. 1(d) by the two data points representing separate deposition runs at $P = 60\,\mathrm{W}$ which differ by only $\Delta\rho = 0.1 \cdot 10^{-4}\,\Omega\,\mathrm{cm}$, a value equal to the measurement limit). Nevertheless, the observed improvement in film resistivity due to the decrease in sputtering power from 125 W to 90 W is not significant with respect to investigated solar cell performance. If considering the corresponding 32 % reduction in the film growth rate (data not presented), we decided to keep $P = 125\,\mathrm{W}$ and $U_b = 25\,\mathrm{V}$ as fixed parameters in all the further-presented experiments with b-ZnO.

The findings discussed above illustrate that the low-voltage RF substrate bias applied to the growing ZnO films is a principal deposition parameter in preparation of highly conductive nominally undoped ZnO films. An operator can thus change the conductivity of a ZnO film from highly resistive to highly conductive in a single depostion step. Consequently, the complete i-/n-doped bilayer can be prepared from a single ZnO target under the condition of maintaining the RF discharge above the growing TCO layer. However, it is also important to mention that the upscaling of the RF substrate biasing in the industrial process is uneasy and may be expensive to implement. The suggested approach has thus a potential to simplify the solar cell fabrication at large manufacturing volumes once the upscaling issue is properly addressed.

Finally, it is to be noted that, in contrast to the ZnO films, we did not observe any significant improvement in AZO films resistivity or NIR transparency that could be related to the RF substrate bias application or sputtering power alteration, as verified in a separate set of experiments.

B. Characterization of conductive b-ZnO films

In the previous section we have identified the optimal deposition conditions at which the resistivity of the b-ZnO films is minimized. In the following we investigate the optical and

electrical properties of the representative b-ZnO and AZO films of comparable thickness ($t \approx 385\,\mathrm{nm}$) and resistivity ($\rho \approx 1.05 \cdot 10^{-3}\,\Omega\,\mathrm{cm}$) that were used in solar cell preparation experiments. All the film characteristics are summarized in Table I together with principal deposition process parameters, including the growth rate r_d. Afterwards, we examine the room-temperature and high temperature stability of selected b-ZnO and AZO films.

Figure 2 presents the transmittance and reflectance spectra of the two layers measured within the 300 nm to 1600 nm region. It can be seen that the UV absorption edge of the AZO film exhibits a shift towards lower wavelengths, due to its higher optical band gap ($E_\mathrm{g} = 3.73\,\mathrm{eV}$ in comparison to 3.43 eV for b-ZnO) caused by stronger Burstein-Moss effect [38, 39]. However, the most significant difference between the two transmittance curves can be observed in the NIR spectral region where a pronounced transmittance drop caused by free-carrier absorption is visible for the AZO film. Instead, the NIR transmittance of the b-ZnO films stays relatively high as the respective plasma wavelength increases by $\Delta\lambda_\mathrm{p} = 400\,\mathrm{nm}$ (from 1774 nm to 2173 nm) with respect to the AZO film.

These latter observations are both indicators of substantially lower free carrier concentration n_e in the b-ZnO film than within the AZO film. Indeed, the Hall measurements confirmed that n_e is about 2.4 times lower ($1.76 \cdot 10^{20}\,\mathrm{cm}^{-3}$ compared to $4.30 \cdot 10^{20}\,\mathrm{cm}^{-3}$). (Nevertheless, it is to be noted that the n_e value of the nominally undoped ZnO reported here is the same [21] or even higher [24, 25] than that of other highly conductive ZnO films in literature). At the other hand, the Hall mobility μ_e of b-ZnO film is significantly higher ($30.4\,\mathrm{cm}^2\mathrm{V}^{-1}\mathrm{s}^{-1}$ compared to $14.0\,\mathrm{cm}^2\mathrm{V}^{-1}\mathrm{s}^{-1}$).

The free carriers in b-ZnO films may be due to native defects such as O vacancies ($\mathrm{V_O}$) or Zn interstitials ($\mathrm{Zn_i}$), and/or due to hydrogen incorporation [18]. However, the SIMS analysis of the films under comparison has eliminated H doping as a principal electron donor; In fact, the average H concentration within the highly conductive b-ZnO and isolating ZnO films differs by only a factor of three, while the charge carrier density is expected to vary by several orders of magnitude. It should be also emphasized that there were no detectable traces of Al and Cu within the b-ZnO films, as verified by SIMS and by separate EDX and XPS analyses. This eliminates the cross-contamination of the ZnO layers by Al from the AZO target or magnetron shields, and by Cu that could originate from the plate on which the ZnO target is bonded.

The environmental stability of the prepared films was investigated in two different ways.

In the first experiment the ambient aging of b-ZnO films was tested. Here, it is to be noted that the average air humidity in Luxembourg region varies in between 70 % (summers) and 90 % (winters) [41]. The film resistivity evolution of a b-ZnO film ($P = 125\,\mathrm{W}$, $U_\mathrm{b} = 25\,\mathrm{V}$, $t = 265\,\mathrm{nm}$) was monitored during the 14 months exposure to air at room temperature, as shown in Fig. 3(a). The change in film resistivity after the first 12 months was very small, $\Delta\rho = 2.2 \cdot 10^{-4}\,\Omega\,\mathrm{cm}$, which represents an increase by only 15 % in comparison to the "as-deposited" film resistance. In addition, we also observed an unexpected drop between the 12^{th} and 13^{th} month of the experiment (corresponding to July-August period when the air humidity is in average the lowest [41]), lowering thus the above-mentioned resistivity rise to only 8 % after the 14 months of "shelve conditions".

In the second experiment numerous single layer and bilayer coatings were tested for their stability at elevated temperature. They were left in an oven filled with air of changing and uncontrolled humidity at 105°C, and their resistivity was measured regularly (at room temperature) during a period of approximately 1900 hours. Fig. 3(b) depicts the results for four selected films: the 390 nm-thick b-ZnO and AZO single layers and two 450 nm-thick n-type window bilayers (ZnO/AZO and ZnO/b-ZnO) that both include a 60 nm underlayer of undoped highly resistive ZnO. It should be stressed that the latter coatings were prepared using the same procedure and experimental conditions as used in the solar cell fabrication experiments.

It can be seen that both b-ZnO and ZnO/b-ZnO films exhibit a comparable rise in their resistivity after approximately 1900 hours of heating: $\Delta\rho \approx 2.5 \cdot 10^{-3}\,\Omega\,\mathrm{cm}$ and $\Delta\rho \approx 3.0 \cdot 10^{-3}\,\Omega\,\mathrm{cm}$, respectively. In constrast, the films containing AZO layer experienced the resistivity rise of only $\Delta\rho \approx 0.5 \cdot 10^{-3}\,\Omega\,\mathrm{cm}$. This observation suggests a faster degradation of b-ZnO layer. Moreover, thinner b-ZnO films showed even a sharper increase in resistivity (results not presented). Nevertheless, it is to be underlined that the observed resistivity value after nearly 2000 hours of continuous heat treatment is still in the range which is sufficient for a proper solar cell functioning.

It is discussed in literature that the water adsorption at grain boundaries is the principal process responsible for the commonly observed increase in Al-doped ZnO films resistivity [42, 43]. With our current experimental set-up we can neither confirm nor discard this degradation mechanism in the case of b-ZnO films under investigation. For this reason, another tests with controlled humidity (damp heat stability or "accelerated ageing") are in

preparation.

C. Characterization of Cu(In,Ga)Se_2, $CuInSe_2$ and $Cu_2ZnSnSe_4$ solar cells

Replacement of the AZO layer by the b-ZnO layer within an n-type window of the low band gap solar cells is supposed to increase its overall quantum efficiency in NIR and thus its short circuit current density. In this section we demonstrate this concept. In particular, we present several examples of thin film solar cells based on Cu(In,Ga)Se_2, $CuInSe_2$ and $Cu_2ZnSnSe_4$ absorbers, and we discuss their characteristics and performance with respect to the effect of the TCO window.

Figure 4 shows the QE spectra and the IV characteristics of the prepared cells, ilustratings in each figure a comparison of results obtained from solar cells based on absorbers fabricated in the same process and covered by an identical CdS buffer layer, but with a different ZnO/TCO window; the first one formed by the standard ZnO/AZO bilayer, and the other one by the ZnO/b-ZnO bilayer. It should be stressed that neither the $CuInSe_2$ nor the $Cu_2ZnSnSe_4$ cells presented here are examples of our best achievable absorbers, but they are the only representatives on which both types of the TCO window were tested. Furthermore, the Cu(In,Ga)Se_2 and $Cu_2ZnSnSe_4$ cells are equipped with an antireflective coating, while the $CuInSe_2$ cells are not. The corresponding solar cell characteristics are summarized in Table II. It is to be noted that the short circuit current derived by integration over the entire QE with an AM 1.5 irradiation spectrum, J_{SC}(QE), and its counterpart obtained from the IV measurements, J_{SC}(IV), do not always agree. We attribute these differences to uncertainties in cell area determination, to variations in shading caused by grids, and to differences in the used irradiation spectra.

Figures 4(a-c) illustrate the effect of the improved transmission of the b-ZnO layer in the NIR region that is also translated into a clearly higher quantum efficiency just above the absorber's band gap. This effect is more pronounced in the QE response of the cells with a lower band gap, and it should as a rule increase their short circuit current. For instance, the J_{SC}(QE) rises by $0.5\,\mathrm{mA\,cm^{-2}}$ in the case of Cu(In,Ga)Se_2 cells ($E_g = 1.11\,\mathrm{eV}$), and by $1.5\,\mathrm{mA\,cm^{-2}}$ for $Cu_2ZnSnSe_4$ cells ($E_g = 0.85\,\mathrm{eV}$). It should be highlighted that a lower QE response in the UV region (where we see the influence of the smaller optical band gap of b-ZnO layer) does not significantly compromise the cell performance, as the loss in the

respective J_{SC}(QE) is only about 0.1 mA cm^{-2}.

In contrast, a notably improved QE response in NIR is not reflected in the J_{SC}(QE) for $CuInSe_2$ cells covered by b-ZnO. This observation can be ascribed mainly to a deep dip in the AM 1.5 spectra that falls into the middle of the spectral region of interest (caused by H_2O absorption and highlighted in grey in Fig. 4(b)), and to the observed differences in the interference pattern visible in the QE spectra ($CuInSe_2$ cells have no antireflective coating). More surprisingly, the corresponding J_{SC}(IV) value does also not reflect the gain in NIR, most probably due to the variations in the grid area and the related shading.

The open circuit voltage V_{OC} does not seem to be significantly affected by the window layer, as the observed differences are within the usual variations between absorbers prepared in the same deposition process. Nevertheless, the efficiency of the Cu(In,Ga)Se_2 and $CuInSe_2$ cells does not increase proportionally to the short circuit current because the fill factor FF tends to decrease. Such a drop in FF could be caused by changes in parasitic resistances and/or diode quality factor (all listed in Table II).

In the following the parasitic resistances are compared in the dark in order to avoid any effect of voltage-dependent photocurrent generation, which would distort the extracted values under irradiation. In contrast, the diode factors are analysed under irradiation because only these respective values can influence FF.

The series resistance R_S is very low for all the cells under investigation, in most cases below 0.5 Ω cm^2. If there is any observable difference between the cells with ZnO/AZO and ZnO/b-ZnO window, the series resistance is lower for those containing b-ZnO, as also verified for several other solar cells (not presented). This finding confirms the excellent conductivity of the b-ZnO layer. In addition, it should be mentioned that all $CuInSe_2$ cells exhibit comparable series resistance after the 6 months period of ambient exposure ($R_S < 0.5\,\Omega\,cm^2$, not shown). These are very encouraging results that will be followed by damp heat stability testing.

Furthermore, there is no observable trend in shunt resistance R_{Sh} in case of the Cu(In,Ga)Se_2 and $CuInSe_2$ cells. In contrast, the $Cu_2ZnSnSe_4$ cells show a higher shunt resistance if covered by a ZnO/b-ZnO bilayer, even though its absolute value is rather low independently on the window type used. At the moment we can only guess that the application of RF bias during conductive b-ZnO deposition may also change some properties of the underlying i-ZnO and/or CdS layer, which could also improve the resulting shunt resistance. In any

case, the changes in both types of the parasitic resistance cannot explain the observed drop in the fill factor.

Instead, it is a higher diode quality factor A that changes substantially when the AZO layer is replaced by b-ZnO. In fact, its value increases for all the solar cells independently of the absorber type: from 1.5 to 2.0 for the $Cu(In,Ga)Se_2$, from 2.7 to 3.4 for the $CuInSe_2$, and from 1.6 to 2.0 for the $Cu_2ZnSnSe_4$. Such a significant increase in the diode factor makes it apparent that the TCO film is not just a conducting contact layer, but also the n-partner of the p/n-junction. As discussed in the previous section, b-ZnO possesses a lower doping level than AZO. When the n-partner has a lower doping level the total charge in the space charge region on the p-side decreases [44]. Since we cannot suppose that the conducting b-ZnO layer has an influence on the doping level of the absorber, the space charge region in the absorber has to be narrower. This is likely to change the details of the recombination paths and thus the diode factor [45]. It should be noted that the above-discussed phenomenon is the least pronounced in the case of $Cu_2ZnSnSe_4$ solar cell, due to the strong effect of the low shunt resistance on the diode factor. It can be speculated that a proper optimisation of the buffer layer can help to rectify the observed trend of increasing A and decreasing FF.

The presented observations indicate that the highly conducting b-ZnO layer can significantly enhance the efficiency of low band gap solar cells as a result of improved short circuit current. Encouraged by these findings we have equipped one of our best $Cu_2ZnSnSe_4$ absorbers with a ZnO/b-ZnO bilayer and an antireflective coating. The resulting solar cells characteristics are shown in Fig. 5. An efficiency of 8.4 % has been achieved, based on a rather high open circuit voltage of 378 mV and a short circuit current of nearly 39 mA cm^{-2}. Both of these values are better than those obtained for our previous cells [27, 46]. We attribute the high V_{OC} to the quality of the absorber and the high J_{SC}(IV) to the elevated transparency of the b-ZnO layer and to the antireflective coating.

IV. CONCLUSIONS

In this contribution we show that the application of the low-voltage substrate RF biasing of the growing ZnO films during the non-reactive sputter deposition makes them as conductive as when doped by aluminium ($\rho \leq 1 \cdot 10^{-3}\,\Omega\,\mathrm{cm}$). This approach can improve the short circuit current and thus the power conversion efficiency of the solar cells with the absorption edge around 1 eV.

First, we describe the deposition conditions at which the resistivity of nominally undoped b-ZnO films is minimized, by identifying the optimal combination of the Ar pressure, the sputtering power and the substrate RF bias voltage. Afterwards, we show that the prepared b-ZnO films exhibit a largely improved optical transmittance in the NIR spectral region in comparison to the AZO films of the same resistivity. The latter observations indicate a substantially lower free carrier concentration ($1.76 \cdot 10^{20}\,\mathrm{cm}^{-3}$ compared to $4.30 \cdot 10^{20}\,\mathrm{cm}^{-3}$) and a higher free carrier mobility ($30.4\,\mathrm{cm}^2\mathrm{V}^{-1}\mathrm{s}^{-1}$ compared to $14.0\,\mathrm{cm}^2\mathrm{V}^{-1}\mathrm{s}^{-1}$), as verified by Hall analysis. We also present that the b-ZnO films exhibit an excellent ambient air stability during a 14 months period, but a slightly lower high temperature stability than AZO films, as suggested by a faster increase in the film resistivity after approximately 1900 hours of heating at 105°C.

Subsequently, we demonstrate that a higher transmission of the b-ZnO layers raises the NIR quantum efficiency of the thin film solar cells based on Cu(In,Ga)Se_2, $CuInSe_2$ and $Cu_2ZnSnSe_4$ absorbers. This results in an increase in the short circuit current by up to $1.5\,\mathrm{mA\,cm}^{-2}$ as illustrated in the case of $Cu_2ZnSnSe_4$ cell with the band gap of 0.85 eV, which as a consequence improves its power conversion efficiency by 0.5 %. On the other hand, we observe a slightly decreased FF in the case of Cu(In,Ga)Se_2 and $CuInSe_2$ cells, most probably due to the lover doping level in b-ZnO. However, we expect to solve this issue by optimising the buffer layer doping. Finally, we report that the best $Cu_2ZnSnSe_4$ absorber covered by a b-ZnO window layer reached J_{SC} of nearly $39\,\mathrm{mA\,cm}^{-2}$ and the respective efficiency of 8.4 %.

ACKNOWLEDGMENTS

The authors wish to thank Mr. Thomas Schuler for his expert technical assistance, Dr. Nathalie Valle for SIMS analyses, Dr. Jérôme Guillot for XPS analyses, and CRP Gabriel Lippmann for the access to the XRD, EDX and profilometry equipment. The financial support of TDK Corporation within the NOTO project and Fond National de la Recherche within the CURI and KITS2 projects are gratefully acknowledged.

---

[1] W. N. Shafarman, S. Siebentritt, and L. Stolt. Cu(InGa)Se_2 Solar Cells. In Handbook of Photovoltaic Science and Engineering, pages 546–599. John Wiley & Sons, Ltd, 2011.

[2] P. Jackson, D. Hariskos, Wuerz R., W. Wischmann, and M. Powalla. Compositional investigation of potassium doped Cu(In,Ga)Se_2 solar cells with efficiencies up to 20.8%. physica status solidi (RRL), 8(3):219–222, 2014.

[3] D. Herrmann, P. Kratzert, S. Weeke, M. Zimmer, J. Djordjevic-Reiss, R. Hunger, L. Bach, P. Lindberg, E. Wallin, O. Lundberg, and L. Stolt. CIGS module manufacturing with high deposition rates and efficiencies. In 40th IEEE Photovoltaic Specialist Conference (IEEE, Denver, 2014), in press.

[4] E. Wallin, U. Malm, T. Jarmar, M. Edoff, O. Lundberg, and L. Stolt. World-record Cu(InGa)Se_2-based thin-film sub-module with 17.4% efficiency. Prog. Photovolt: Res. Appl., 20(7):851–854, 2012.

[5] W. Wang, M. T. Winkler, O. Gunawan, T. Gokmen, T. Todorov, Y. Zhu, and D. B. Mitzi. Device Characteristics of CZTSSe Thin-Film Solar Cells with 12.6% Efficiency. Adv. Energy Mater., 2013.

[6] A. E. Delahoy and S. Guo. Transparent conducting oxides for photovoltaics. In Handbook of Photovoltaic Science and Engineering, pages 716–796. John Wiley & Sons, Ltd, 2011.

[7] G. Brammertz, Y. Ren, M. Buffière, S. Mertens, J. Hendrickx, H. Marko, A. E. Zaghi, N. L., C. Köble, J. Vleugels, M. Meuris, and J. Poortmans. Electrical characterization of $Cu_2ZnSnSe_4$ solar cells from selenization of sputtered metal layers. Thin Solid Films, 535(0):348 – 352, 2013.

[8] I. L. Repins, M. J. Romero, J. V. Li, Su-Huai Wei, D. Kuciauskas, Chun-Sheng Jiang, C. Beall,

C. DeHart, J. Mann, Wan-Ching H., G. Teeter, A. Goodrich, and R. Noufi. Kesterite Successes, Ongoing Work, and Challenges: A Perspective From Vacuum Deposition. IEEE J. Photovolt., 3(1):439–445, Jan 2013.

[9] A. Redinger, M. Mousel, M. H. Wolter, N. Valle, and S. Siebentritt. Influence of S/Se ratio on series resistance and on dominant recombination pathway in $Cu_2ZnSn(SSe)_4$ thin film solar cells. Thin solid films, 535:291–295, 2013.

[10] Y. Aida, V. Depredurand, J. K. Larsen, H. Arai, D. Tanaka, M. Kurihara, and S. Siebentritt. Cu-rich $CuInSe_2$ solar cells with a Cu-poor surface. Prog. Photovolt: Res. Appl., 2014.

[11] T. Bertram, V. Deprédurand, and S. Siebentritt. In-Se surface treatment of Cu-rich grown $CuInSe_2$. In 40th IEEE Photovoltaic Specialist Conference (IEEE, Denver, 2014), in press.

[12] T. J. Coutts, J. S. Ward, D. L. Young, K. A. Emery, T. A. Gessert, and R. Noufi. Critical issues in the design of polycrystalline, thin-film tandem solar cells. Prog. Photovolt: Res. Appl., 11(6):359–375, 2003.

[13] T. J. Coutts, K. A. Emery, and J. S. Ward. Modeled performance of polycrystalline thin-film tandem solar cells. Prog. Photovolt: Res. Appl., 10(3):195–203, 2002.

[14] S. Nishiwaki, S. Siebentritt, P. Walk, and M. Ch. Lux-Steiner. A stacked chalcopyrite thin-film tandem solar cell with 1.2 V open-circuit voltage. Prog. Photovolt: Res. Appl., 11(4):243–248, 2003.

[15] S. Calnan, H.M. Uphadhyaya, S. Buecheler, G. Khrypunov, A. Chirila, A. Romeo, R. Hashimoto, T. Nakada, and A.N. Tiwari. Application of high mobility transparent conductors to enhance long wavelength transparency of the intermediate solar cell in multi-junction solar cells. Thin Solid Films, 517(7):2340 – 2343, 2009. Thin Film Chalogenide Photovoltaic Materials (EMRS, Symposium L).

[16] T. Minami, T. Miyata, and J. Nomoto. Impurity-doped ZnO Thin Films Prepared by Physical Deposition Methods Appropriate for Transparent Electrode Applications in Thin-film Solar Cells. IOP Conference Series: Materials Science and Engineering, 34(1):012001, 2012.

[17] K. Ellmer and G. Vollweiler. Electrical transport parameters of heavily-doped zinc oxide and zinc magnesium oxide single and multilayer films heteroepitaxially grown on oxide single crystals. Thin Solid Films, 496(1):104 – 111, 2006. Proceedings of the Fourth International Symposium on Transparent Oxide Thin Films for Electronics and Optics (TOEO-4).

[18] K. Ellmer. Electrical properties. In Ellmer K., Klein A., and Rech B., editors, Transparent

Conductive Zinc Oxide: Basics and Applications in Thin Film Solar Cells, pages 34–78. Springer, Berlin, 2008.

[19] T.A. Gessert, J. Burst, X. Li, M. Scott, and T.J. Coutts. Advantages of transparent conducting oxide thin films with controlled permittivity for thin film photovoltaic solar cells. Thin Solid Films, 519(21):7146–7148, 2011. Proceedings of the EMRS 2010 Spring Meeting Symposium M: Thin Film Chalcogenide Photovoltaic Materials.

[20] T. Minami, H. Nanto, and S. Takata. Highly conductive and transparent zinc oxide films prepared by rf magnetron sputtering under an applied external magnetic field. Appl. Phys. Lett., 41(10):958–960, 1982.

[21] T. Minami, H. Sato, K. Ohashi, T. Tomofuji, and S. Takata. Conduction mechanism of highly conductive and transparent zinc oxide thin films prepared by magnetron sputtering. J. Cryst. Growth, 117(1-4):370–374, 1992.

[22] D. K. Murti. Substrate biased RF sputtering of zinc oxide films. Applications of Surface Science, 11/12:308 – 314, 1982.

[23] M. J. Brett, R. W. McMahon, J. Affinito, and R. R. Parsons. High rate planar magnetron deposition of transparent, conducting, and heat reflecting films on glass and plastic. J. Vac. Sci. Technol. A, 1(2):352–355, 1983.

[24] J. B. Webb, D. F. Williams, and M. Buchanan. Transparent and highly conductive films of zno prepared by rf reactive magnetron sputtering. Appl. Phys. Lett., 39(8):640–642, 1981.

[25] Andrea Illiberi, Frank Grob, Corne Frijters, Paul Poodt, Ram Ramachandra, Hans Winands, Marcel Simor, and Pieter Jan Bolt. High rate (7nm/s), atmospheric pressure deposition of zno front electrode for cu(in,ga)se2 thin-film solar cells with efficiency beyond 15 Prog. Photovolt: Res. Appl., 21(8):1559–1566, 2013.

[26] K. Sakurai, R. Hunger, R. Scheer, C. A. Kaufmann, A. Yamada, T. Baba, Y. Kimura, K. Matsubara, P. Fons, H. Nakanishi, and S. Niki. In situ diagnostic methods for thin-film fabrication: utilization of heat radiation and light scattering. Prog. Photovolt: Res. Appl., 12(2-3):219–234, 2004.

[27] A. Redinger, J. Sendler, R. Djemour, T. P. Weiss, G. Rey, P. J. Dale, and S. Siebentritt. Different bandgaps in $Cu_2ZnSnSe_4$; A high temperature coevaporation study. Journal of Photovoltaics, submitted.

[28] A. M. Gabor, J. R. Tuttle, D. S. Albin, M. A. Contreras, R. Noufi, and A. M. Hermann.

High-efficiency $CuIn_xGa_{1-x}Se_2$ solar cells made from $(In_x,Ga_{1-x})_2Se_3$ precursor films. Applied Physics Letters, 65:198–200, 1994.

[29] M. A. Contreras, B. Egaas, K. Ramanathan, J. Hiltner, A. Swartzlander, F. Hasoon, and R. Noufi. Progress toward 20% effciency in $Cu(In,Ga)Se_2$ polycrystalline thin-film solar cells. Prog. Photovolt: Res. Appl., 7:311–316, 1999.

[30] V. Deprédurand, D. Tanaka, Y. Aida, M. Carlberg, N. Fèvre, and S. Siebentritt. Current loss due to recombination in Cu-rich $CuInSe_2$ solar cells. J. Appl. Phys., 115(4), 2014.

[31] L. J. van der Pauw. A Method of Measuring the Resistivity and Hall Coefficient on Lamellae of Arbitrary Shape. Philips Technical Review, 20(8):220–224, 1858/59.

[32] W.E. Vargas, D.E. Azofeifa, and N. Clark. Retrieved optical properties of thin films on absorbing substrates from transmittance measurements by application of a spectral projected gradient method. Thin Solid Films, 425(1-2):1–8, 2003.

[33] W. E. Vargas and D. Castro. Closed equation for the normal incidence reflectance of thin films on absorbing substrates. Appl. Opt., 46(4):502–505, 2007.

[34] N. W. Ashcroft and N. D. Mermin. Solid state Physics. Saunders, 1976.

[35] J. I. Langford and A. J. C. Wilson. Scherrer after sixty years: A survey and some new results in the determination of crystallite size. J. Appl. Cryst., 11(2):102–113, 1978.

[36] Ellmer K. and Klein A. ZnO and Its Applications. In Ellmer K., Klein A., and Rech B., editors, Transparent Conductive Zinc Oxide: Basics and Applications in Thin Film Solar Cells, pages 1–33. Springer, Berlin, 2008.

[37] A. R. Burgers, J. A. Eikelboom, A. Schonecker, and W. C. Sinke. Improved treatment of the strongly varying slope in fitting solar cell I-V curves. In Photovoltaic Specialists Conference, 1996., Conference Record of the 25th IEEE, pages 569–572, 1996.

[38] E. Burstein. Anomalous Optical Absorption Limit in InSb. Phys. Rev., 93:632–633, 1954.

[39] G. Sanon, R. Rup, and A. Mansingh. Band-gap narrowing and band structure in degenerate tin oxide (SnO_2) films. Phys. Rev. B, 44:5672–5680, 1991.

[40] G. Rey, C. Ternon, M. Modreanu, X. Mescot, V. Consonni, and D. Bellet. Electron scattering mechanisms in fluorine-doped SnO_2 thin films. J. Appl. Phys., 114(18):183713, 2013.

[41] Wikipedia. accessed: 01/09/2014.

[42] T. Tohsophon, J. Hpkes, S. Calnan, W. Reetz, B. Rech, W. Beyer, and N. Sirikulrat. Damp heat stability and annealing behavior of aluminum doped zinc oxide films prepared by mag-

netron sputtering. Thin Solid Films, 511512(0):673 – 677, 2006. EMSR 2005 - Proceedings of Symposium F on Thin Film and Nanostructured Materials for Photovoltaics.

[43] D. Greiner, S.E. Gledhill, Ch. Kble, J. Krammer, and R. Klenk. Damp heat stability of al-doped zinc oxide films on smooth and rough substrates. Thin Solid Films, 520(4):1285 – 1290, 2011. Transparent Conductive Materials (TCM 2010).

[44] S. M. Sze and Kwok K. Ng. Physics of Semiconductor Devices, chapter 2. John Wiley and Sons, 1991.

[45] A. L. Fahrenbruch and R. H. Bube. Fundamentals of Solar Cells, chapter 5. Academic Press, New York, London, 1983.

[46] M. Mousel, T. Schwarz, R. Djemour, T. P. Weiss, J. Sendler, J. C. Malaquias, A. Redinger, O. Cojocaru-Mirédin, P. Choi, and S. Siebentritt. Cu-Rich Precursors Improve Kesterite Solar Cells. Adv. Energy Mater., 4:1300543, 2014.

TABLE I. Selected growth and film characteristics of the two representative b-ZnO and AZO layers used in solar cell fabrication experiments.

Film material		AZO	b-ZnO
P	(W)	140	125
U_b	(V)	0	25
r_d	($\mathrm{nm\,s^{-1}}$)	0.08	0.05
t	(nm)	376	395
ρ	($10^{-3}\,\Omega\,\mathrm{cm}$)	1.03	1.06
E_g	(eV)	3.73	3.43
λ_p	(nm)	1774	2173
n_e	($10^{20}\,\mathrm{cm^{-3}}$)	4.30	1.76
μ_e	($\mathrm{cm^2V^{-1}s^{-1}}$)	14.0	30.4

TABLE II. Selected parameters of the two $Cu(In,Ga)Se_2$, two $CuInSe_2$ and two $Cu_2ZnSnSe_4$ solar cells prepared with ZnO/b-ZnO or ZnO/AZO bilayer as their TCO window. Short circuit current density J_{SC}(IV), open circuit voltage V_{OC}, fill factor FF and efficiency Eff (IV) values are obtained directly from the IV characterization, while J_{SC}(QE) values are enumerated by integrating the QE spectra multiplied by 1.5 AM irradiation. The active area efficiency Eff (QE) is then calculated as $J_{SC}(QE) \cdot V_{OC} \cdot FF$. Series and parallel parasitic resistances R_S and R_{Sh} were evaluated under dark conditions, and the diode quality factors A under irradiation.

Absorber material		$Cu(In,Ga)Se_2$		$CuInSe_2$		$Cu_2ZnSnSe_4$	
TCO film		AZO	b-ZnO	AZO	b-ZnO	AZO	b-ZnO
J_{SC}(IV)	($mA\,cm^{-2}$)	37.9	38.3	37.0	37.2	35.2	37.6
J_{SC}(QE)	($mA\,cm^{-2}$)	37.5	38.0	37.6	37.7	35.1	36.5
V_{OC}	(mV)	664	657	327	321	336	338
FF	(%)	76	72	52	47	58	58
Eff	(IV) (%)	19.2	18.2	6.3	5.7	6.9	7.4
Eff	(QE) (%)	18.9	18.0	6.4	5.7	6.8	7.2
R_S	($\Omega\,cm^{-2}$)	0.6	0.3	0.3	0.2	0.3	0.3
R_{Sh}	($\Omega\,cm^{-2}$)	10200	9470	1000	860	80	205
A		1.5	2.0	2.7	3.4	1.6	2.0

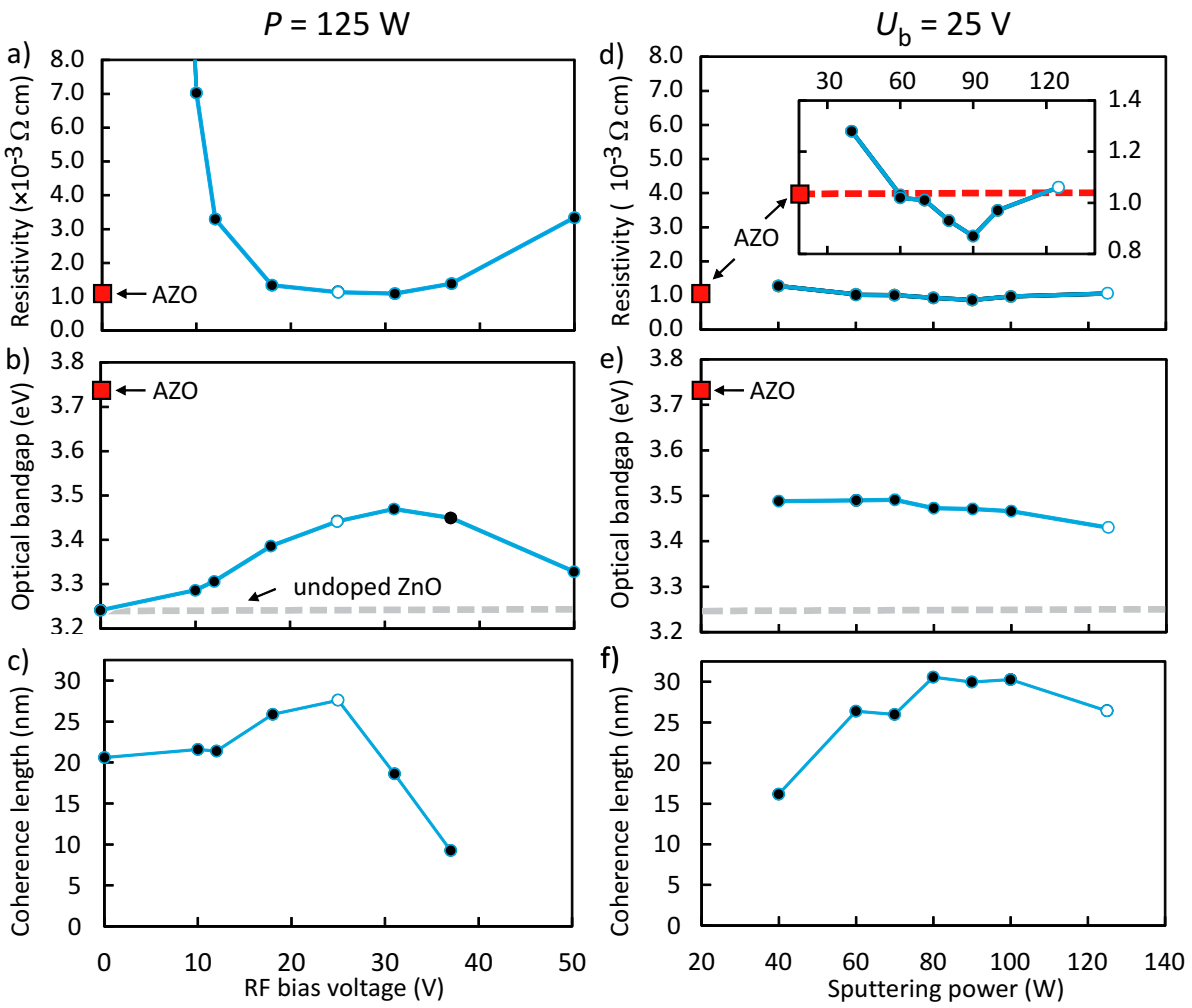

FIG. 1. b-ZnO film resistivity (a,d), the optical band gap (b,e), and the X-ray coherence length in a perpendicular direction to film plane (c,f). Figures (a-c) illustrate the experiments in which the sputtering power was fixed to $P = 125\,\mathrm{W}$ and the negative substrate RF bias voltage U_b was varied, while figures (d-f) depict the experiments with variable P and fixed $U_\mathrm{b} = 25\,\mathrm{V}$. Open symbols identify the b-ZnO film deposited at $P = 125\,\mathrm{W}$ and $U_\mathrm{b} = 25\,\mathrm{V}$, the conditions used in preparation of solar cells. The resistivity and band gap values of a reference AZO (ZnO:Al 98:2 at%) film are also highlighted in red in (a,d) and (b,e), and the optical band gap of pure ZnO is marked in grey in (b) and (e). A magnified view of the resistivity values is depicted in the insert of (d).

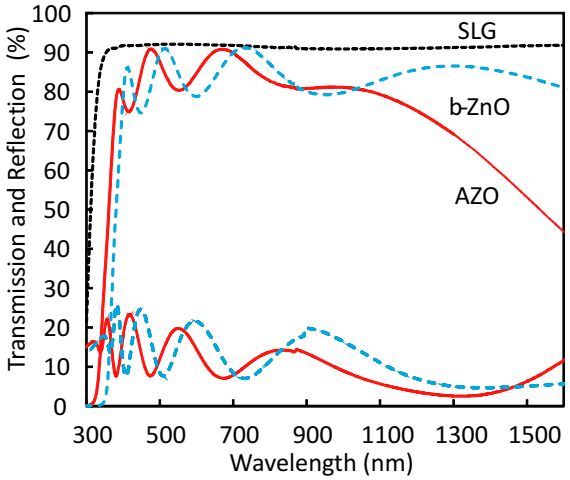

FIG. 2. Optical transmission spectra (higher curves) and the reflection spectra (lower curves) of the representative b-ZnO and AZO layers, accompanied by the transmission of an SLG glass substrate.

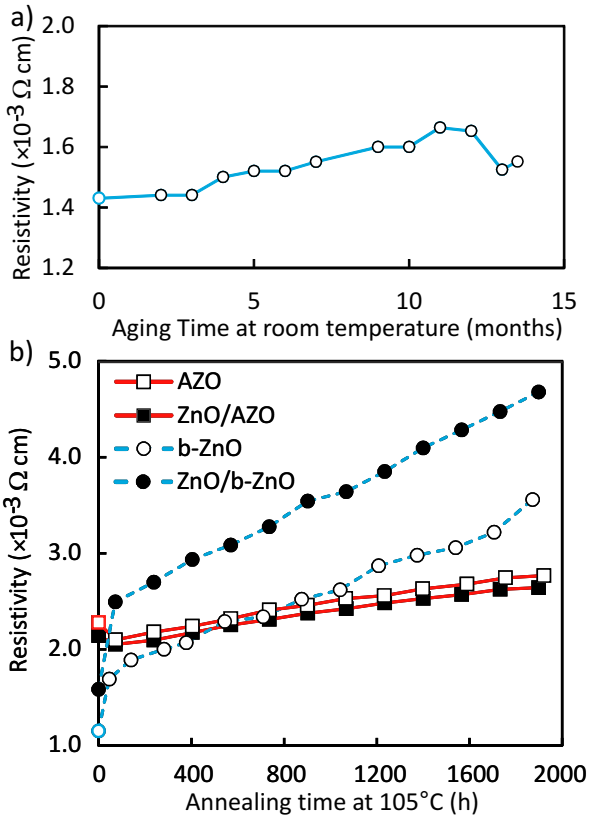

FIG. 3. Film resistivity monitored as a function of time during 14 months exposure to air at room temperature for a b-ZnO single layer (a), and during 1900 hours of annealing in air at 105°C for AZO and b-ZnO single layers, and for ZnO/AZO and ZnO/b-ZnO bilayers (b).

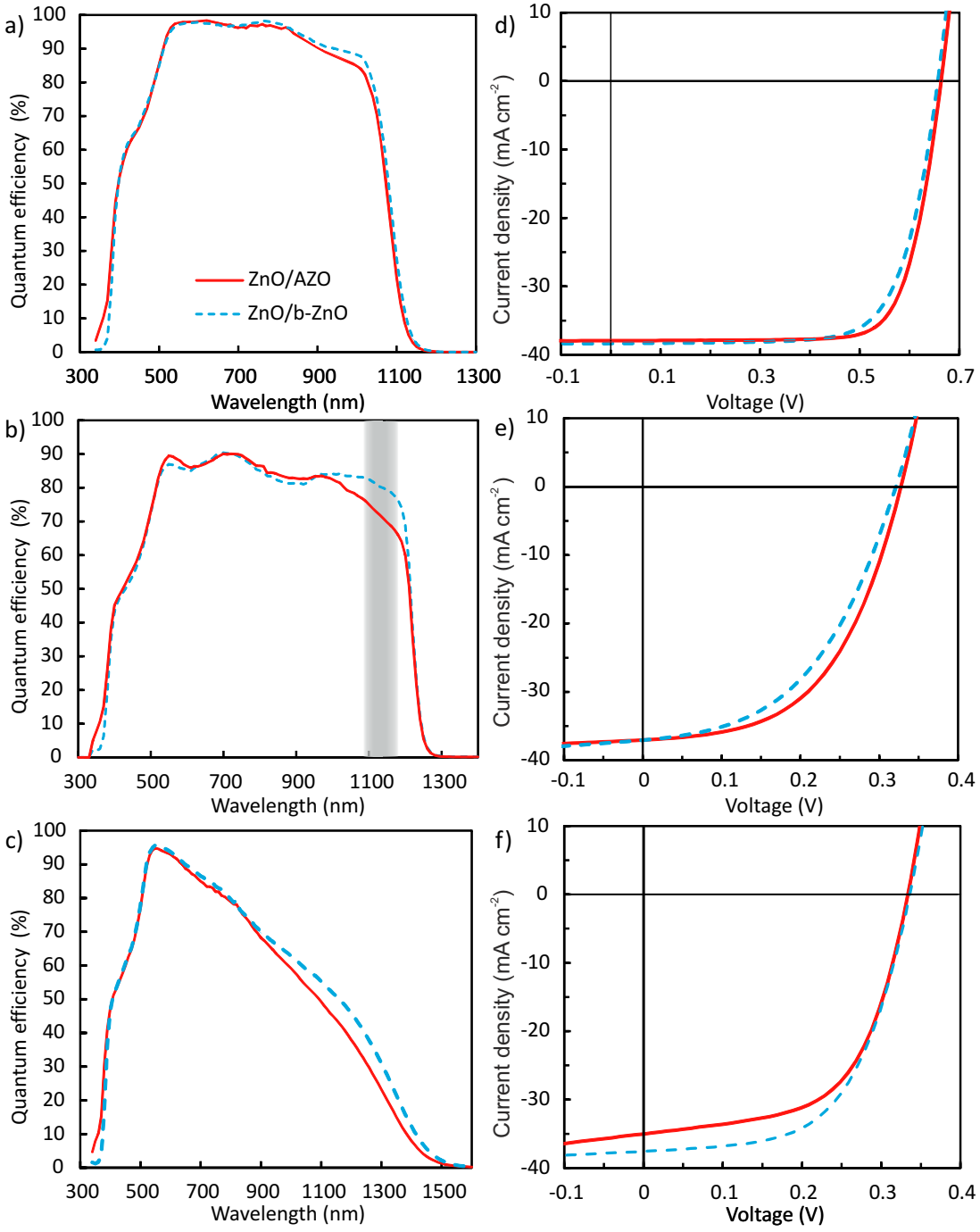

FIG. 4. External quantum efficiency spectra (a,b,c) and I-V characteristics under irradiation (d,e,f) of the three types of solar cells with the TCO window formed by either a ZnO/AZO bilayer, or a ZnO/b-ZnO bilayer. These cells are based on $Cu(In,Ga)Se_2$ (a,d), $CuInSe_2$ (b,e), or $Cu_2ZnSnSe_4$ (c,f) absorbers. The $Cu(In,Ga)Se_2$ and the $Cu_2ZnSnSe_4$ cells were coated with an antireflective coating. The grey area in (b) highligths the deep H_2O absorption region in the AM 1.5 spectrum.

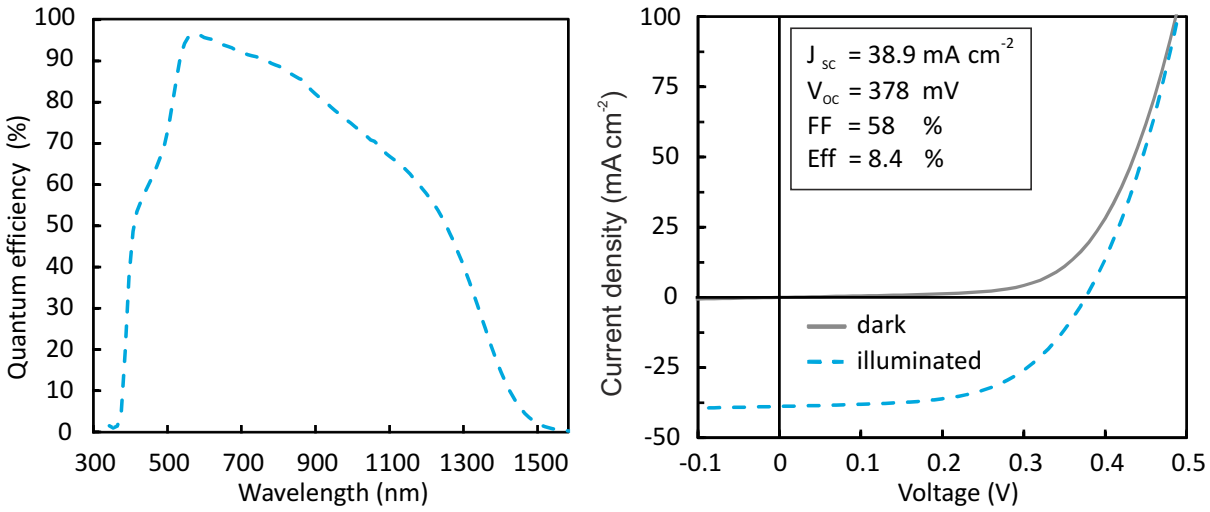

FIG. 5. External quantum efficiency spectra (a) and I-V characteristics in dark and under irradiation (b) of the best $Cu_2ZnSnSe_4$ cell coated with the TCO window formed by a ZnO/b-ZnO bilayer and with an antireflective coating. The principal solar cell parameters are shown in (b).